

Supplementary Information

Self-assembly of PS-PNaSS-PS triblock copolymers from solution to solid state

Sabrina Nehache¹, Mona Semsarilar^{1*}, Martin In², Philippe Dieudonné-George², Joséphine Lai-Kee-Him³, Patrick Bron³, Denis Bouyer¹, André Deratani¹, Damien Quemener^{1*}

¹ Institut Européen des Membranes, IEM, UMR 5635, Université de Montpellier, ENSCM, CNRS, Place Eugène Bataillon, 34095 Montpellier Cedex 05, France.

² Laboratoire Charles Coulomb UMR 5221, Université de Montpellier & CNRS, F-34095, Montpellier, France.

³ Centre de Biochimie Structurale, CNRS UMR 5048, INSERM U1054, Université de Montpellier, Montpellier, France.

* To whom correspondence should be addressed:

Email: damien.quemener@umontpellier.fr; mona.semsarilar@umontpellier.fr

Contents of Supplementary Information:

1. Experimental section
2. Supplementary Scheme 1
3. Supplementary Table 1
4. Supplementary Figures 1-26
5. References

1. Experimental section:

Materials

All reagents were purchased from Sigma-Aldrich and were used as received unless otherwise stated. Azobisisobutyronitrile (AIBN) was purchased from Fluka Chemika and was recrystallized from methanol. Styrene (S) was passed through basic alumina prior to use. Deuterated Chloroform (CDCl_3) and Dimethylsulfoxide ($(\text{CD}_3)_2\text{SO}$) were purchased from Eurisotop.

Synthetic procedure

Synthesis of polystyrene-*b*-poly(sodium 4-styrenesulfonate)-*b*-polystyrene triblock copolymer ($\text{PS}_{96}\text{-PNaSS}_{97}\text{-PS}_{96}$).

The RAFT synthesis of $\text{PS}_{96}\text{-PNaSS}_{97}\text{-PS}_{96}$ was performed in two steps (Supplementary Scheme 1). Styrene was polymerized using DTTC as the chain transfer agent (CTA) and AIBN as the free radical initiator (CTA/initiator molar ratio = 1: 0.5) in bulk. A small amount of 1, 4-dioxane solvent was used to ensure complete dissolution of the CTA. The reaction was stopped after 20 hours (50% conversion, calculated by ^1H NMR (Supplementary Fig. 1), targeting a M_n of 20,000 $\text{g}\cdot\text{mol}^{-1}$). The resulting PS macro-CTA was purified by precipitation in methanol. The SEC analysis in THF suggested a \bar{D} of 1.1 and M_n of 20,100 $\text{g}\cdot\text{mol}^{-1}$ (Supplementary Fig. 2). The second step was performed under a similar RAFT polymerization conditions. The synthesized PS_{192} macro-CTA was dissolved in DMF along with Sodium 4-styrenesulfonate (NaSS) and AIBN. The macro-CTA/initiator molar ratio was fixed at 1:0.25, and NaSS polymerization was conducted at 70°C for 14 hours (100% conversion, target $M_n = 20,000 \text{ g}\cdot\text{mol}^{-1}$). The resulting $\text{PS}_{96}\text{-PNaSS}_{97}\text{-PS}_{96}$ was purified by dialysis against water. As the final synthesized triblock copolymer was not soluble in common SEC eluents (THF, DMF, water), a shorter molecular weight ($\text{PS}_{48}\text{-PNaSS}_{24}\text{-PS}_{48}$)

was synthesized to check the control over the polymerization. The narrow \bar{M}_w of 1.2 (determined by SEC using DMF as eluent) suggests a good control over the polymerization (Supplementary Fig. 3). A DOSY NMR analysis was performed in DMSO- d_6 to confirm the blocking (Supplementary Fig. 4).

Calculation of the Flory–Huggins parameter (χ).

The χ parameter of the system polystyrene-solvent mixture has been estimated in order to better understand the polystyrene block solubility in the initial solution as well as during the evaporation based on the modeling of the solvent composition paths. The Flory–Huggins parameter (χ) was estimated from ¹:

$$\chi = 0.34 + \frac{v_0}{RT} (\delta_{polymer} - \delta_{solvent})^2$$

where R and T are the gas constant and absolute temperature respectively. v_0 was taken to be 97.8 cm³/mol. The solubility parameter δ was taken to be 18.61 MPa^{1/2} for THF, 47.86 MPa^{1/2} for water, and 19.6 MPa^{1/2} for PS. The solubility parameters of the solvent mixture were calculated from the volume-average values of the individual solvents.

Modeling of mass and heat transfers during evaporation.

A ternary polymer system was considered in this model: THF/water/polymer. Both THF and water were assumed to evaporate until the film solidification. The geometry for mass transfer in this system corresponded to the experimental conditions of the film formation. One-directional diffusion along the vertical axis was assumed in the model, thus neglecting boundary effects (the high ratio surface/film thickness validates this assumption). The gas phase next to the top side of the polymer solution was characterized by its temperature T^∞ (gas temperature) and relative humidity (RH). The solubility data of the mixture THF/water was found in the literature². The values of the partial pressure at the upper interface were therefore determined at each time, depending on the local composition and temperature. Because of the low polymer concentration at the beginning of the process, those solubility

data were assumed not to be strongly affected by the polymer. The mass transfer model also relies on the following assumptions: (i) no transfer of polymer in the air, (ii) ideal gas behavior in the gas phase, (iii) gas-liquid equilibrium at the film/air interface, (iv) binary diffusion between water and THF, thus neglecting the presence of the polymer, (v) no excess of volume due to mixing. Based on these assumptions, the continuity equation for water and THF evaporation from the polymer solution can be written along the vertical axis. Because of mass exchanges between the polymer system and the external environment, a coordinate transform was done to fix the boundaries between 0 and 1, therefore the continuity equation can be derived as follows:

$$\frac{\partial \rho_i}{\partial t} - \frac{X}{H(t)} \frac{\partial H(t)}{\partial t} \frac{\partial \rho_i}{\partial X} - \frac{D}{H(t)^2} \left(- \frac{\partial \rho_i}{\partial X} \right) = 0 \quad \text{for } i = 1, 2 \quad (1)$$

The subscripts 1 and 2 were used for water and THF, respectively. D represents the mutual diffusion coefficient between THF and water and ρ_i is the mass concentration of component i . Initial and boundary conditions were applied, depending on the operating conditions. At the air/solution interface, Neumann conditions were considered to take into account water and THF evaporation:

$$X = 1, - \frac{D}{H(t)} \frac{\partial \rho_i}{\partial X} = J_{ig} = k_1 \left(\rho_{ig}^i(T^i) - \rho_{ig}^\infty(T^\infty) \right) \quad \text{for } i = 1, 2 \quad (2)$$

where $\rho_{ig}^i(T^i)$ is the water mass concentration in gas phase at the air/solution interface and $\rho_{ig}^\infty(T^\infty)$ is the water mass concentration in gas phase. k_i represents the mass transfer coefficient.

The water concentration in gas phase bulk (ρ_{1g}^∞) can be deduced from the RH in the bulk and the water concentration at the air/solution interface (ρ_{1g}^i) depends on the water activity a_i and partial pressure of component i . The position of the air/solution boundary $H(t)$, i.e. the solution thickness, can be calculated from the mass transfer flux in the gas phase of component i (J_i^g) using the following ordinary differential equation:

$$\frac{dH(t)}{dt} = \frac{\sum_i J_i^g}{\rho_p} \quad (3)$$

where ρ_p is the polymer solution density.

The mutual diffusion coefficient D involved in equation 2 is calculated at each time step from diffusion data obtained in literature³. Its value depends on (i) the relative concentration of water and (ii) the temperature. Since evaporation is endothermic and since the evaporation of THF is very rapid, a heat transfer model was coupled to the mass transfer model. Because of the geometry involved in this modeling problem, i.e. thin film with an initial thickness less than 15 μm , the heat transfer was simulated using a lumped parameter approach: it was assumed that no temperature gradient was expected to appear during the process, despite the high mass exchanges expected to occur during the initial stage of the evaporation process. The heat flux was therefore assumed to be modeled by the following equation:

$$\frac{dT}{dt} = - \left[\frac{h_{up}(T^\infty - T) + h_{down}(T^\infty - T) + \sum_i J_i^g \Delta H v_i}{\rho_p C p_p H(t)} \right] \quad (4)$$

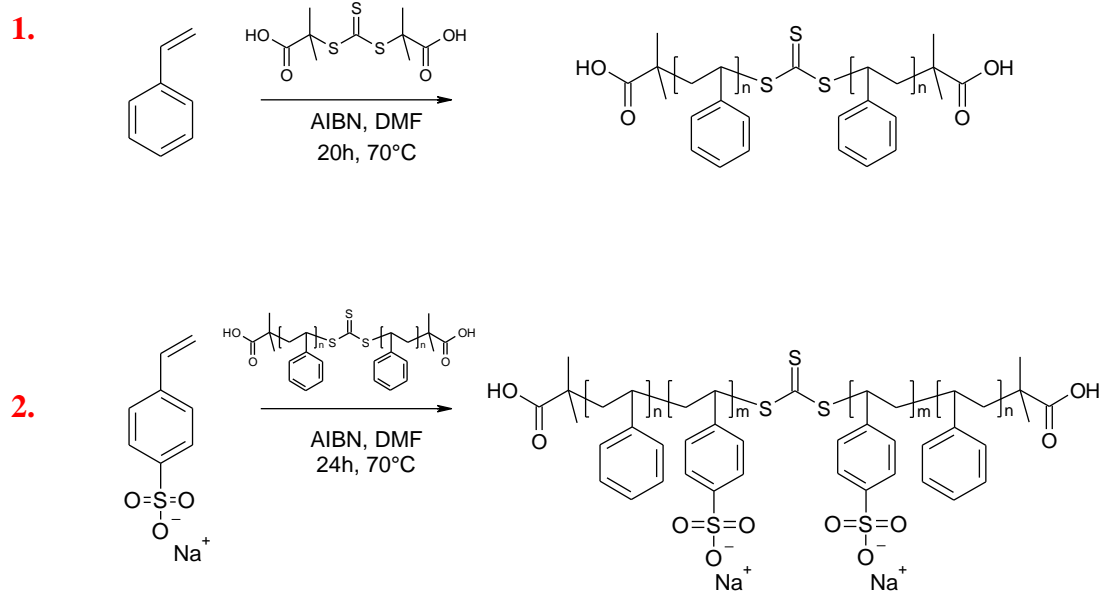
where $\Delta H v_i$ represents the vaporization enthalpy of component i , $H(t)$ is the thickness of the polymer solution at time t and $C p_p$ is the specific heat capacity of the polymer solution. h_{up} and h_{down} represent the heat transfer coefficient at the upper and lower boundary of the system, respectively. The external mass transfer coefficients were calculated by empirical correlations derived in free convection to represent the experimental conditions of membrane formation. Free convection involves air motion that is induced by a density change in the vicinity of the air/solution interface, and the following correlation was used to express the mass transfer coefficient k_i :

$$\frac{k_i L_c y_{air,lm}}{D_{ig}} = 0.816 (Gr Sc_i)^{0.2} \quad (5)$$

where $y_{air,lm}$ is the log mean mole fraction difference of air, D_{ig} is the mutual diffusion coefficient of component i in the air-solvent system, L_c is the characteristic length of the

solution surface. The Grashof number (Gr) allows calculating free convection due to density difference caused by composition gradients and temperature gradients near the air/solution interface and the Schmidt number (Sc_i) depends on fluid properties.

2. Supplementary Scheme 1:



Scheme 1. Synthesis of the triblock copolymer PS₉₆-PNaSS₉₇-PS₉₆ by RAFT polymerization.

3. Supplementary Table 1:

Table S1. PS₉₆-PNaSS₉₇-PS₉₆ solution composition and estimation of $\chi_{\text{PS-solvent}}$ (see Supplementary Methods for the details of calculation).

Samples	Water content (wt.%)	THF/water weight ratio	δ (MPa^{1/2})	$\chi_{\text{PS-solvent}}$
1	3.1	30.0	19.45	0.34
2	5.9	15.0	20.25	0.36
3	11.1	7.50	21.71	0.52
4	15.8	5.00	23.02	0.81
5	27.3	2.50	26.28	2.13
6	38.5	1.50	29.49	4.27
7	46.7	1.10	31.87	6.38
100% THF	0	-	18.61	0.38
100% Water	100	-	47.86	32.38

4. Supplementary Figures:

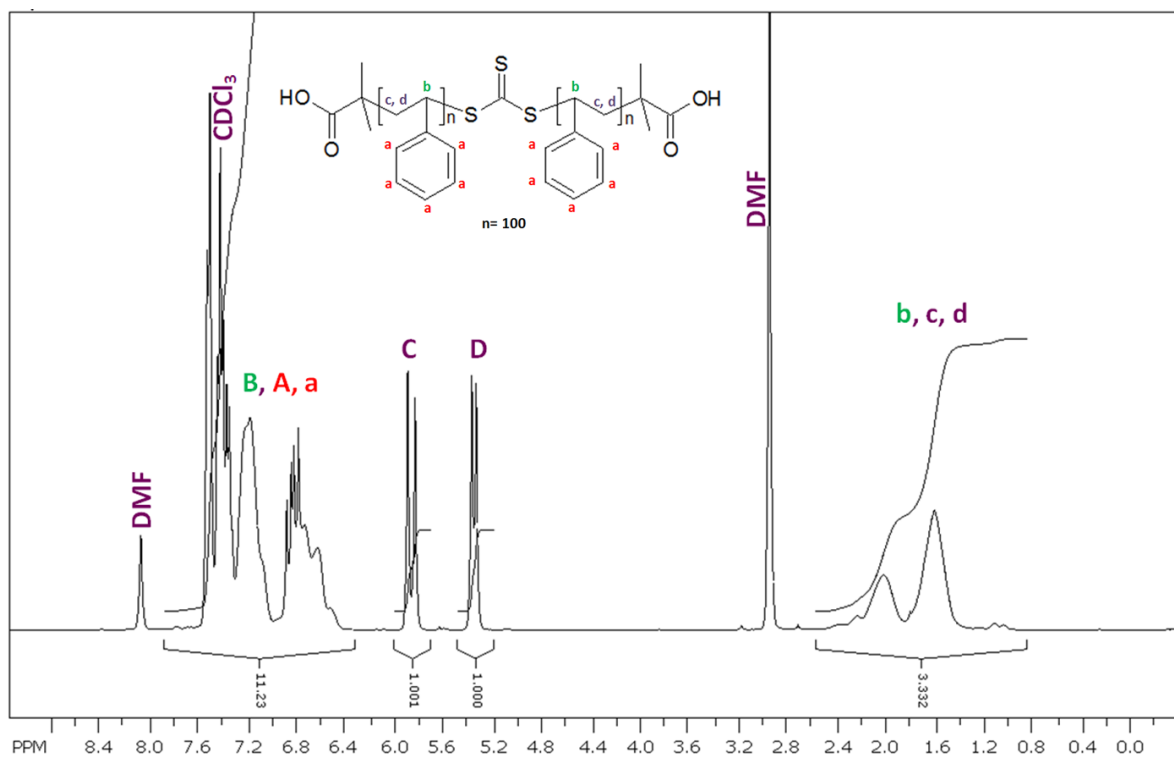


Figure S1. ¹H NMR spectra of PS Macro CTA recorded in CDCl₃ before purification for monomer conversion calculation by comparing the protons of the vinyl (C and D) to the protons of polymer backbone b, c, and d.

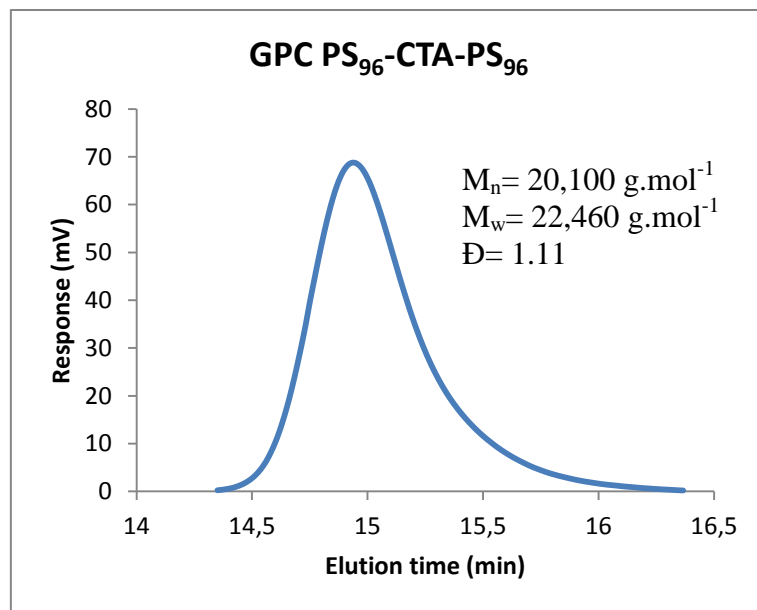


Figure S2. GPC trace of PS Macro-CTA in THF. Polystyrene standards were used for calibration.

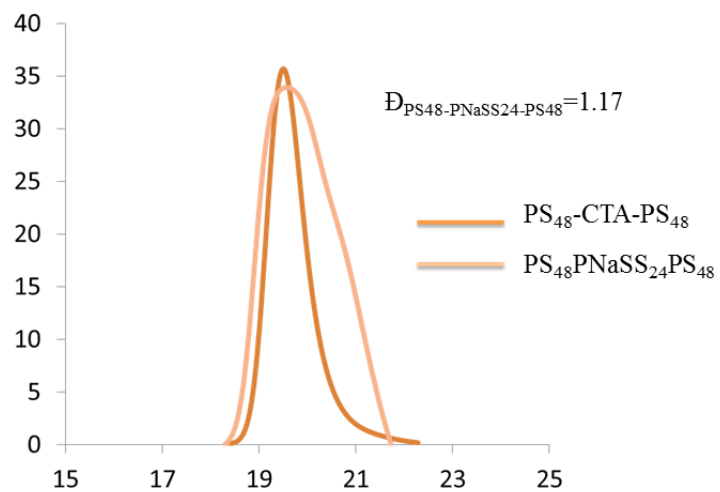


Figure S3. GPC trace of triblock copolymer PS₄₈PNaSS₂₄PS₄₈ versus PS₄₈-CTA-PS₄₈ in DMF. Poly(methyl methacrylate) (PMMA) standards were used for calibration.

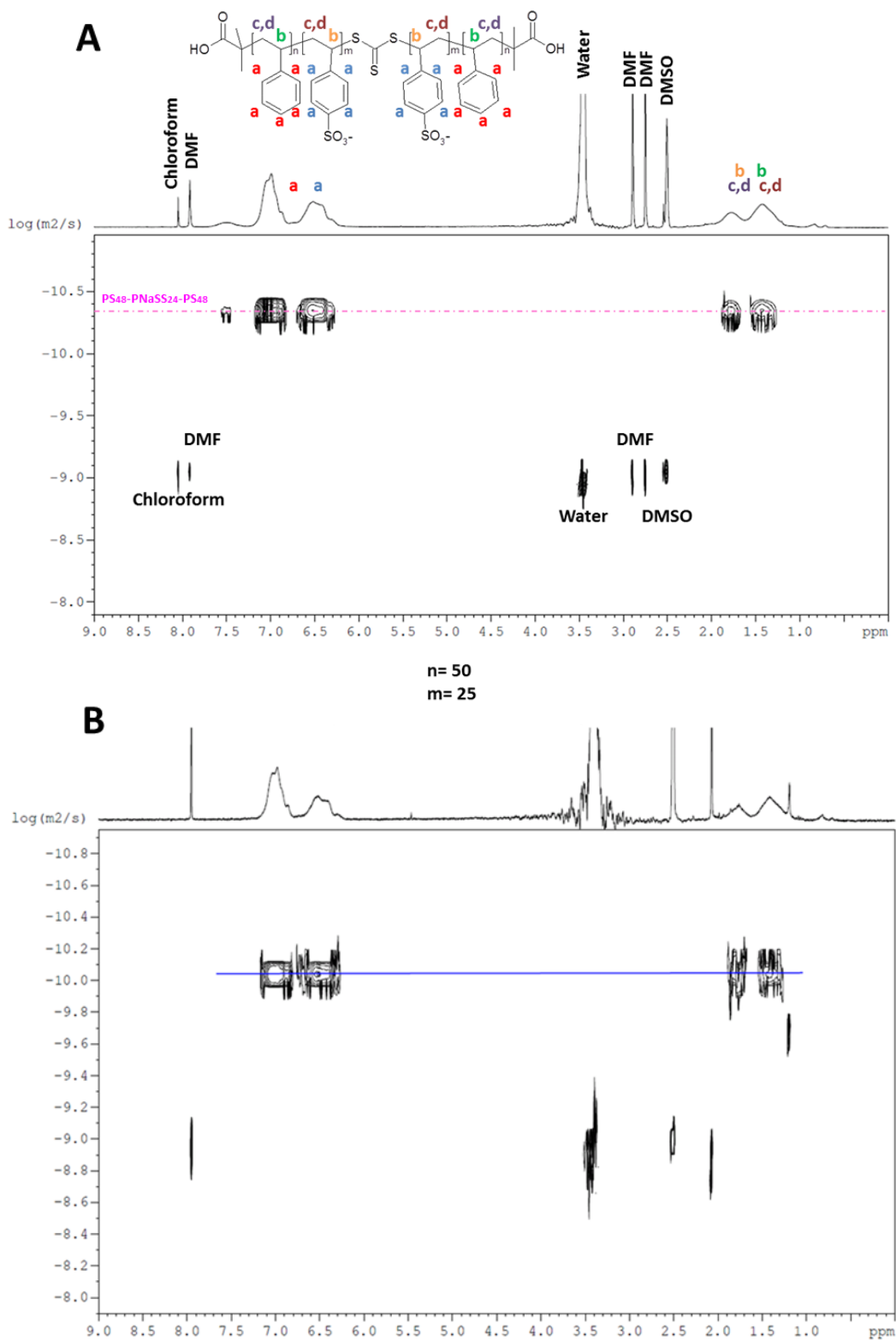


Figure S4. 2D DOSY NMR spectra obtained at 298 K in DMSO-d₆ solution of the copolymer PS₄₈-PNaSS₂₄-PS₄₈ (A) and the PS macro-CTA PS₄₈-CTA-PS₄₈ (B).

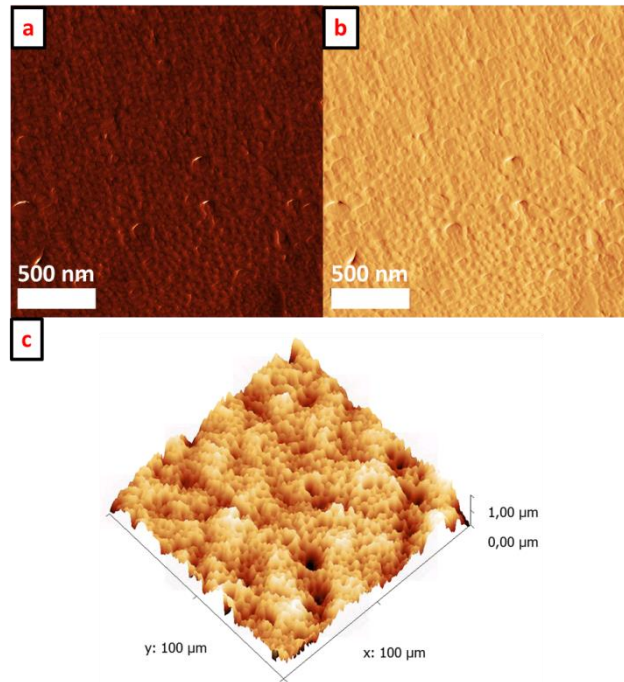


Figure S5. AFM images of thin films prepared from sample 1 via spin-coating (a) Phase image (b) Amplitude (c) 3D view of the topography.

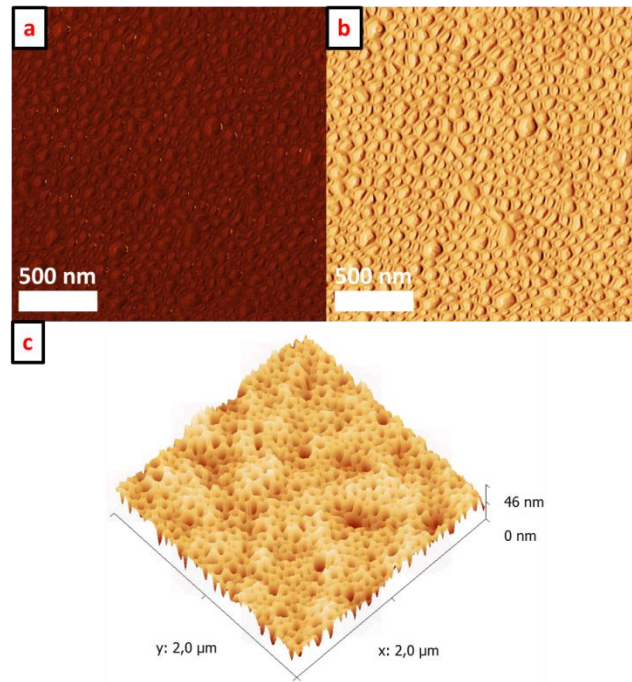


Figure S6. AFM images of thin films prepared from sample 2 via spin-coating (a) Phase image (b) Amplitude (c) 3D view of the topography.

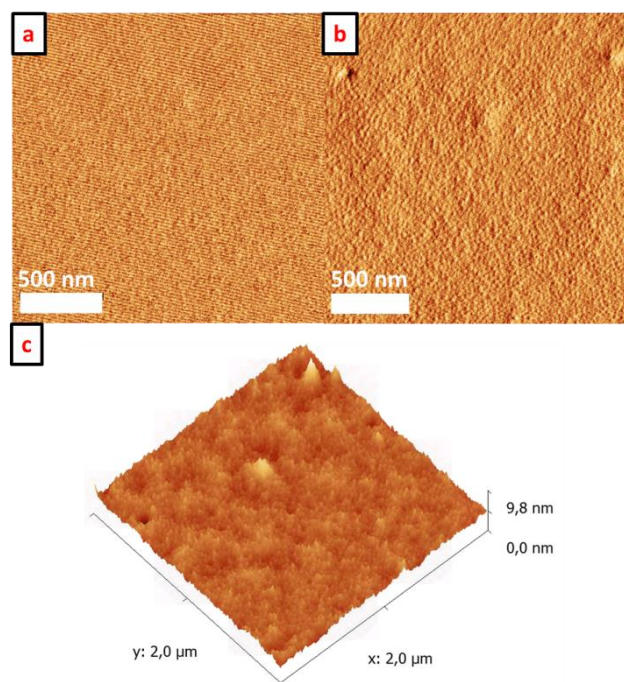


Figure S7. AFM images of thin films prepared from sample 6 via spin coating (a) Phase image (b) Amplitude (c) 3D view of the topography.

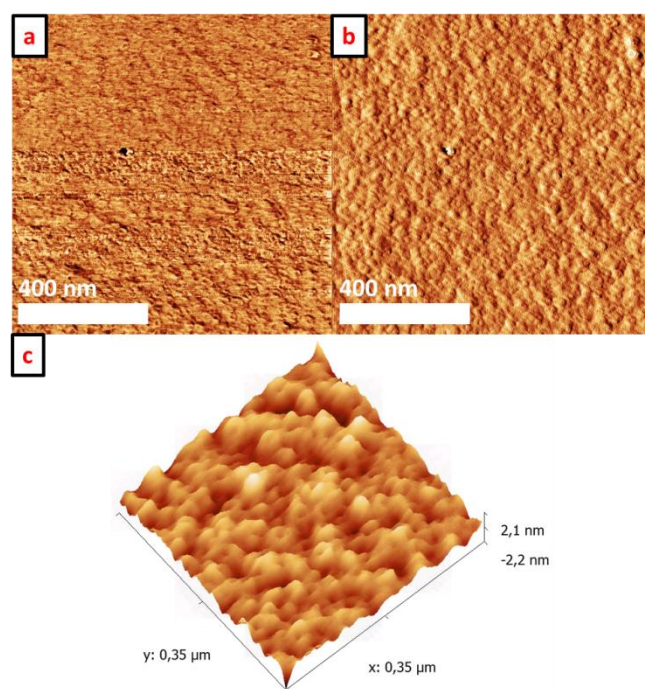


Figure S8. AFM images of thin films prepared from sample 7 via spin-coating (a) Phase image (b) Amplitude (c) 3D view of the topography.

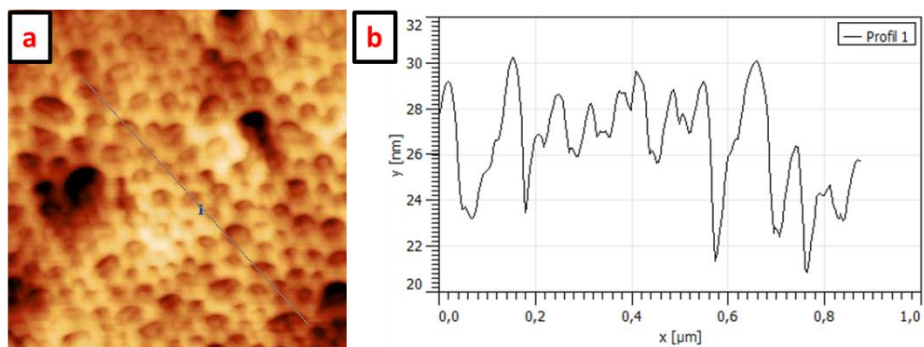


Figure S9. (a) Zoomed AFM topography image of sample 1 (b) Cross-sectional profile of the topography along the line shown in (a). Picture size: 0.9 μm *0.9 μm .

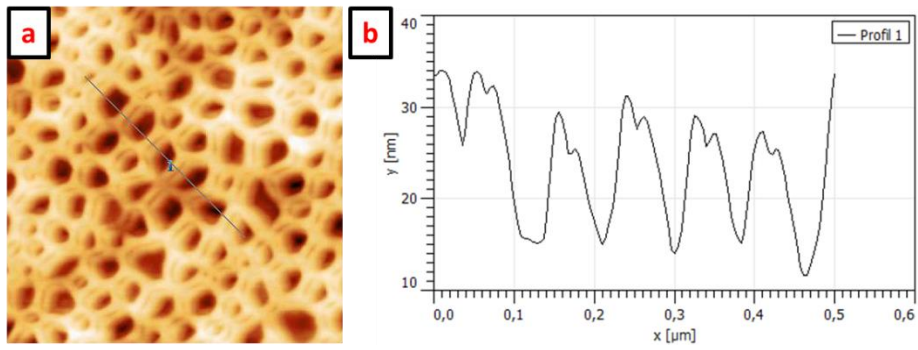


Figure S10. (a) Zoomed AFM topography image of sample 2 (b) Cross-sectional profile of the topography along the line shown in (a). Picture size: $0.75 \mu\text{m} \times 0.75 \mu\text{m}$.

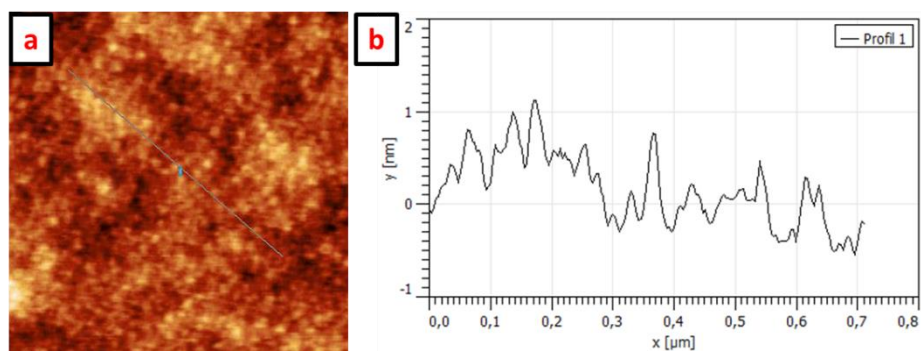


Figure S11. (a) Zoomed AFM topography image of sample 6 (b) Cross-sectional profile of the topography along the line shown in (a). Picture size: 0.85 μm *0.85 μm .

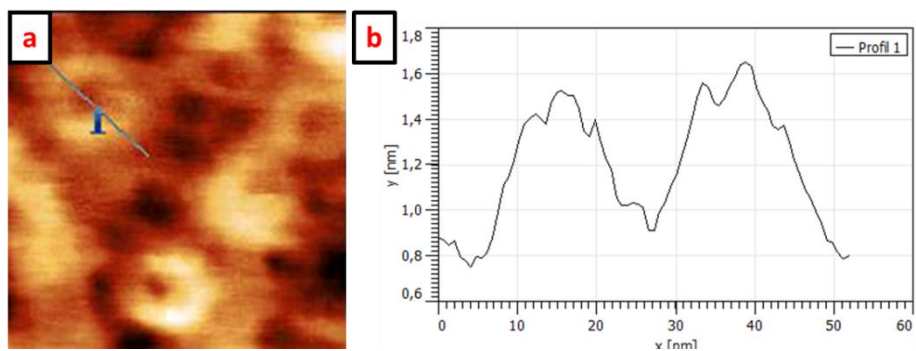


Figure S12. (a) Zoomed AFM topography image of sample 7 (b) Cross-sectional profile of the topography along the line shown in (a). Picture size: $0.12\ \mu\text{m} \times 0.12\ \mu\text{m}$.

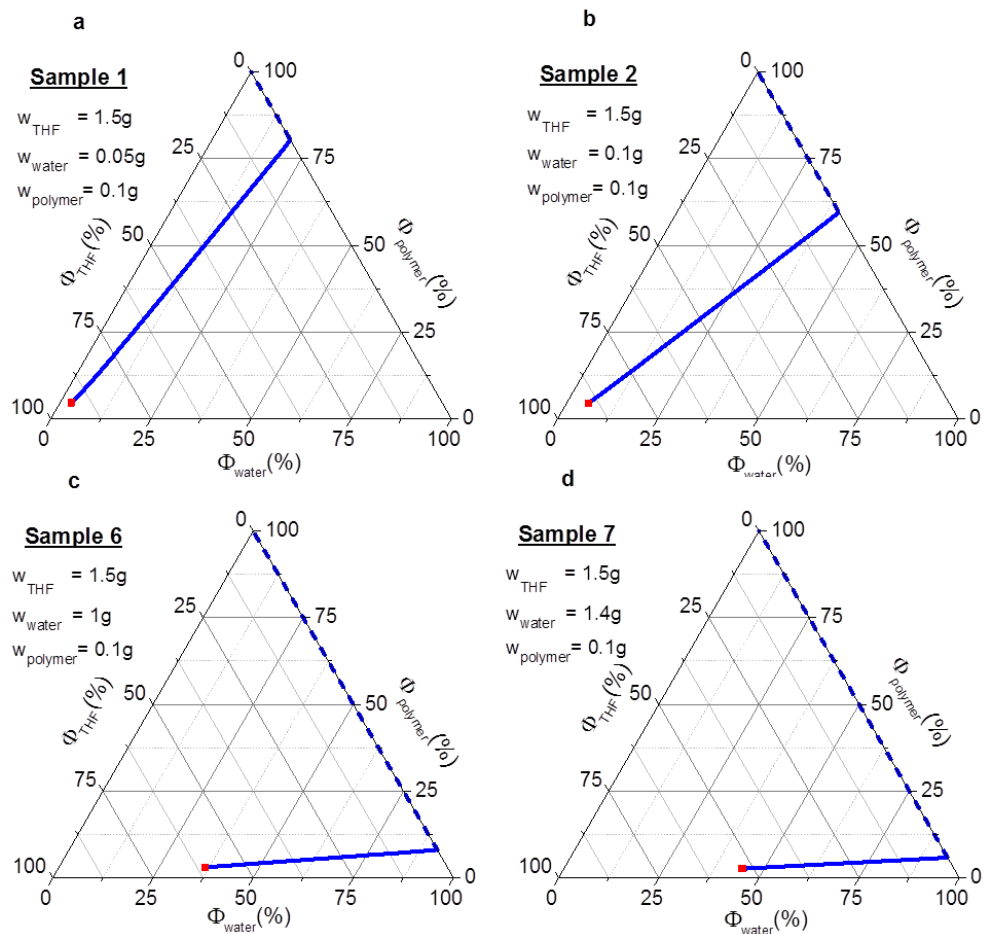


Figure S13. Modeling of the evolution of the solvent composition upon drying (solid blue lines). The red squares symbolize the initial solvent compositions. The dashed blue lines represent the evolution for the binary mixture polymer-water after THF evaporation.

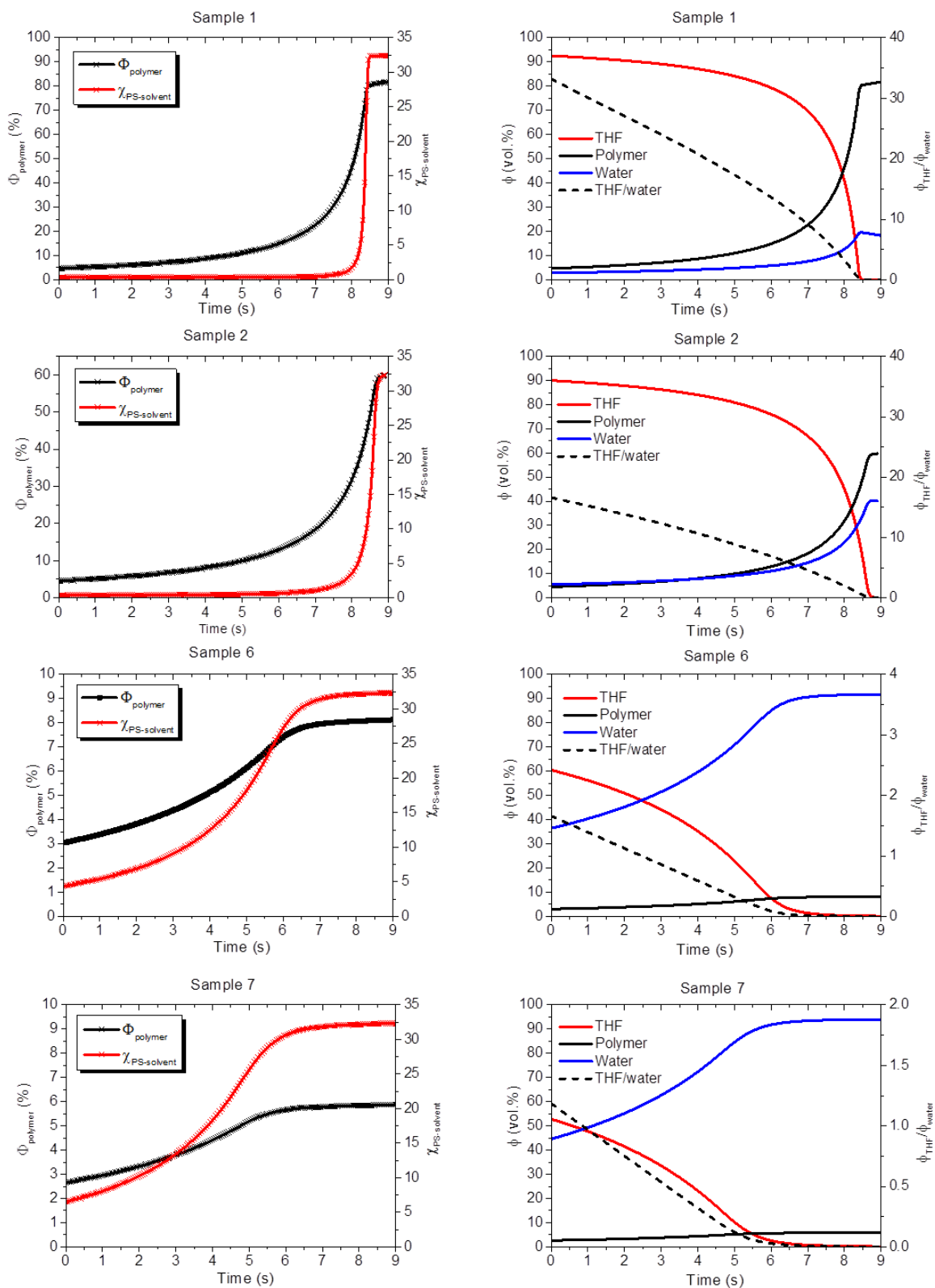


Figure S14. Evolution of the Flory–Huggins parameter ($\chi_{PS-solvent}$) and the solution composition (ϕ) versus the time of drying based on the solvent composition modeling.

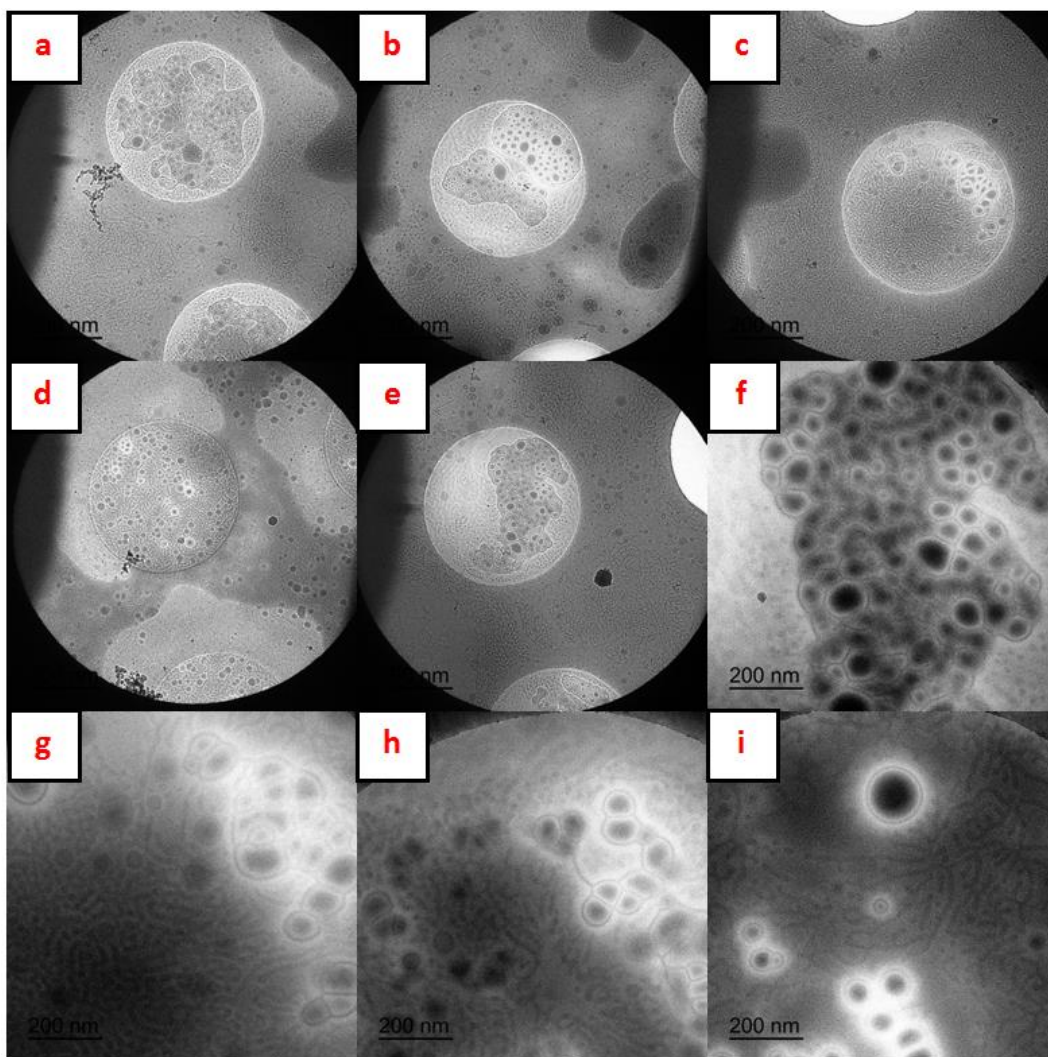


Figure S15. Cryo-TEM images of sample 2 in solution. Coexistence of large compound vesicles, vesicles, worms and spheres.

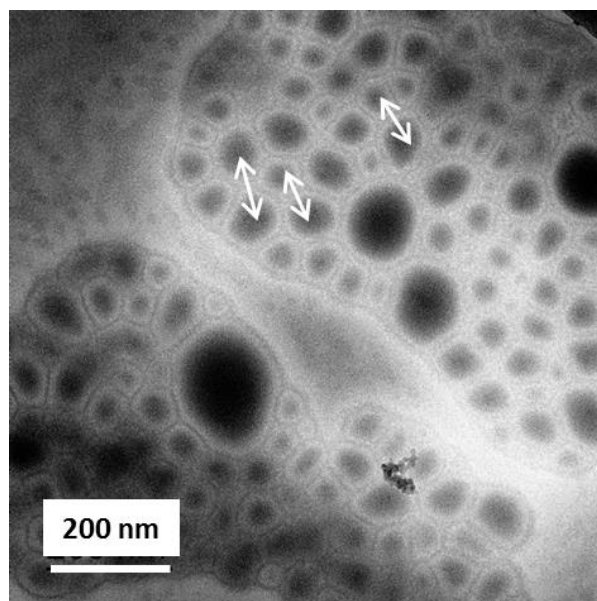


Figure S16. Cryo-TEM image of sample 2 solution. The white arrows indicate the length of center-to-center between two compartments in a large compound vesicle.

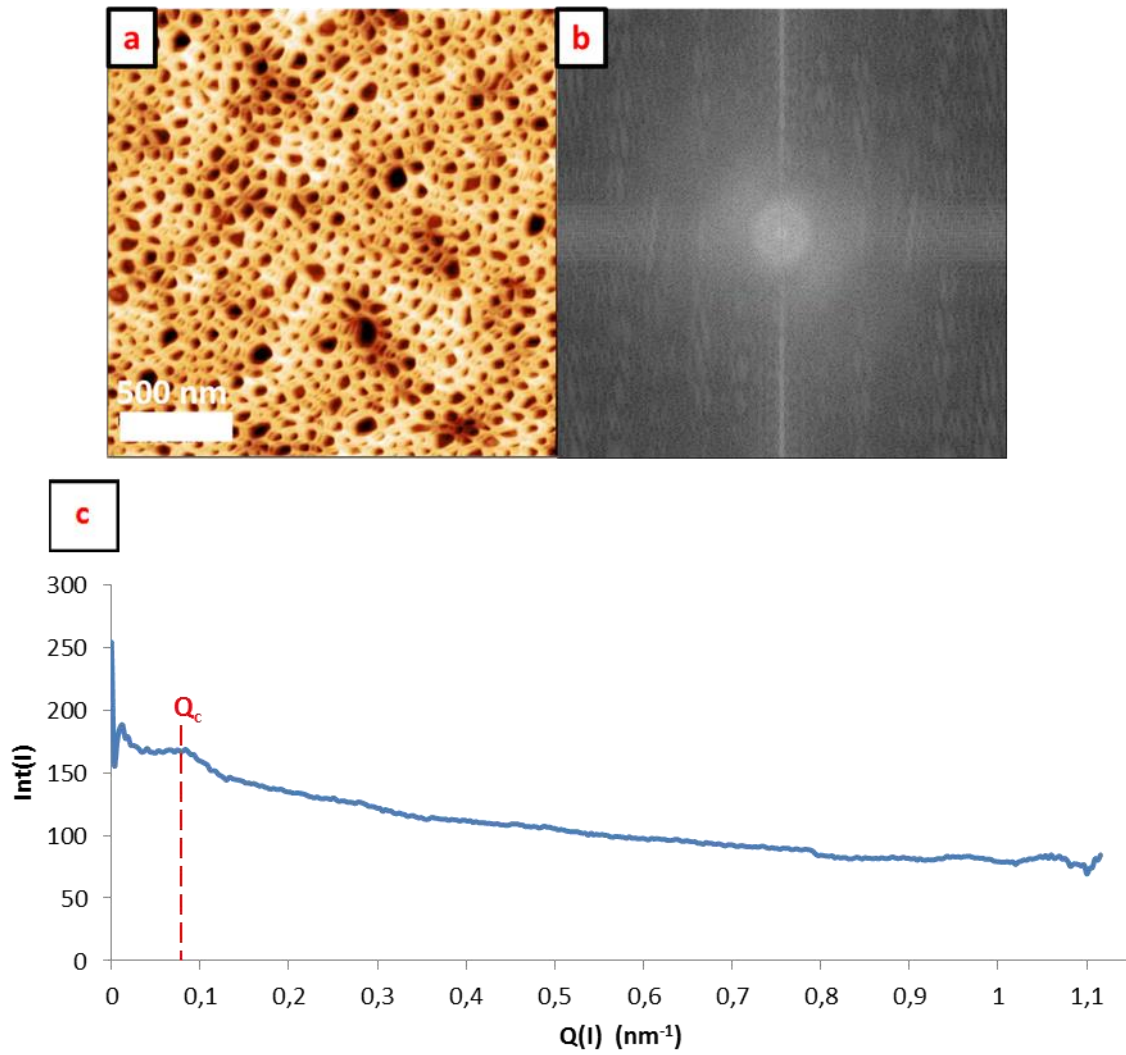


Figure S17. (a) Topography AFM image of sample 2 after spin-coating (b) The corresponding FFT.

(c) Mathematic treatment of FFT (obtained from circular mean) on sample 2 topography image. $Q_c =$

$0,074 \text{ nm}^{-1}$. The characteristic length L_c was calculated according to $L_c = \frac{2\pi}{Q_c} = 85 \text{ nm}$

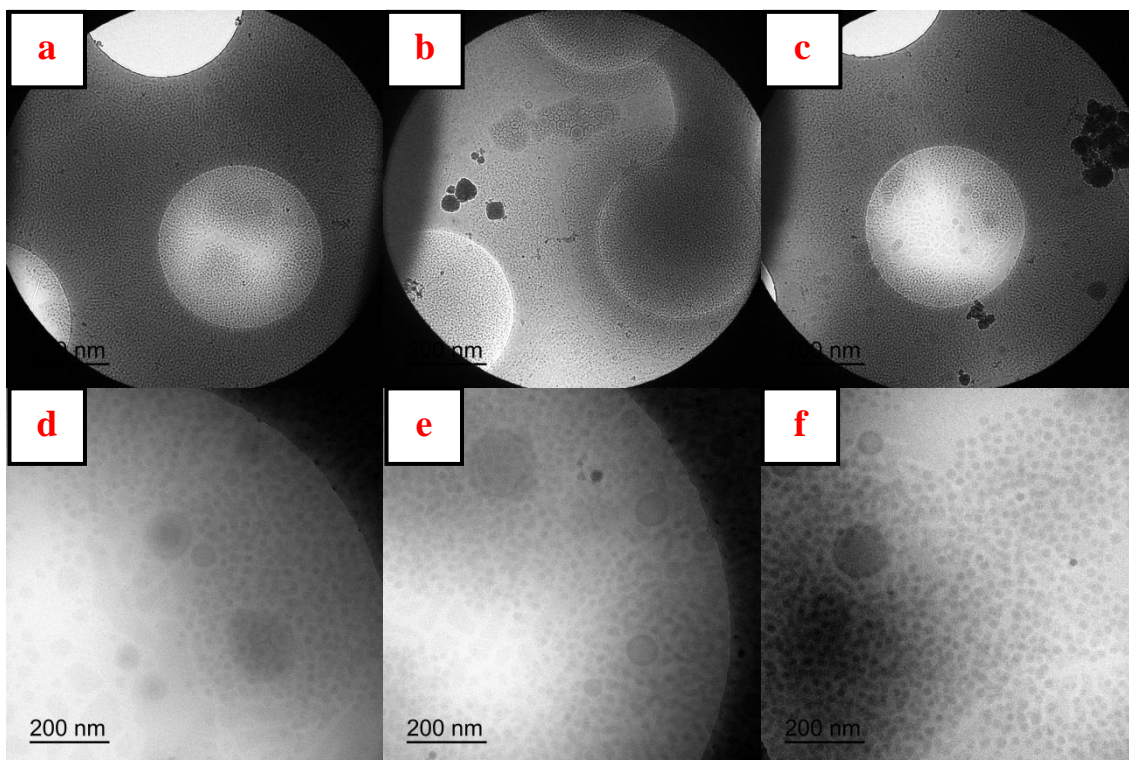


Figure S18. Cryo-TEM images of diluted sample 2 ($C_{\text{polymer}}=2,85$ wt.%; THF/water =15) showing the predominance of spheres with the presence of few vesicles.

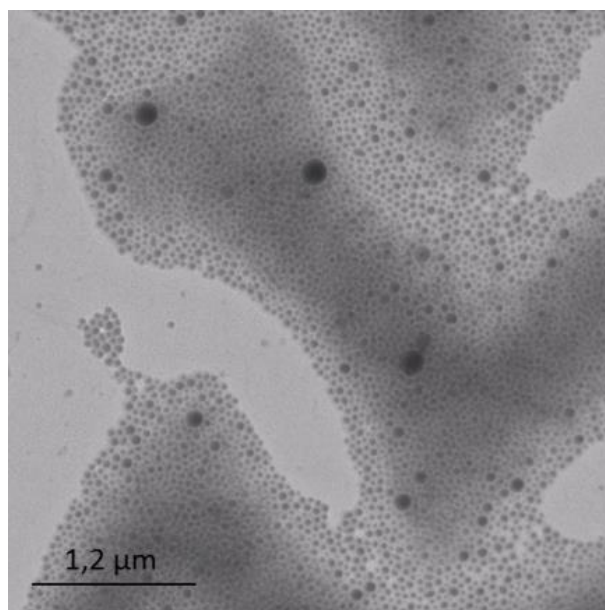


Figure S19. TEM image of sample 2 ($C_{\text{polymer}} = 5.88 \text{ wt.}\%$; THF/water =15) spin-coated on a TEM grid.

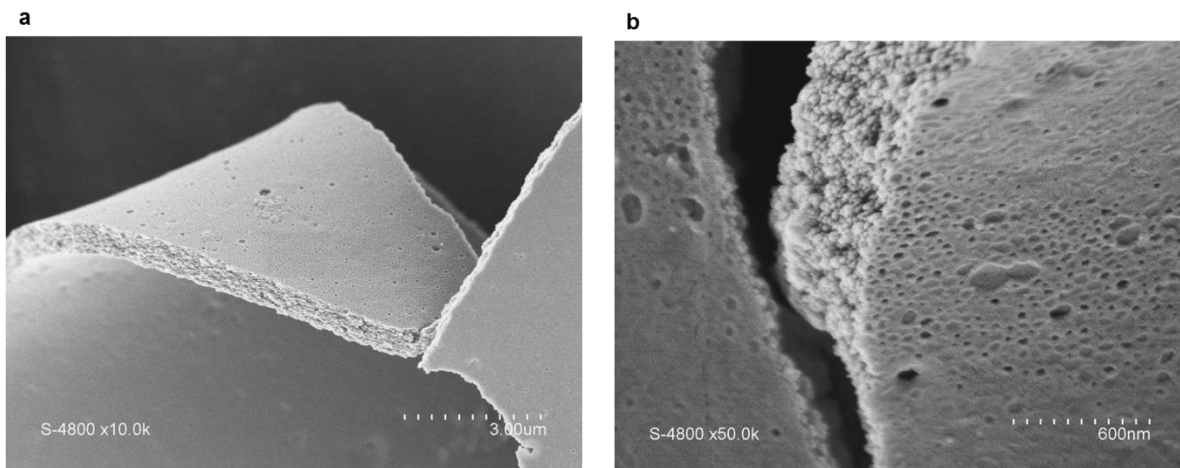


Figure S20. SEM images of sample 2 spin-coated on silicon wafer, dried and detached via immersion in water (a) Top surface, cross-section and bottom surface (b) Bottom surface and cross-section. The bottom surface porosity seems lower, possibly due to the some affinity between the PS chains and the silicon wafer which could induce the formation of a preferential PS wetting onto the silicon wafer⁴.

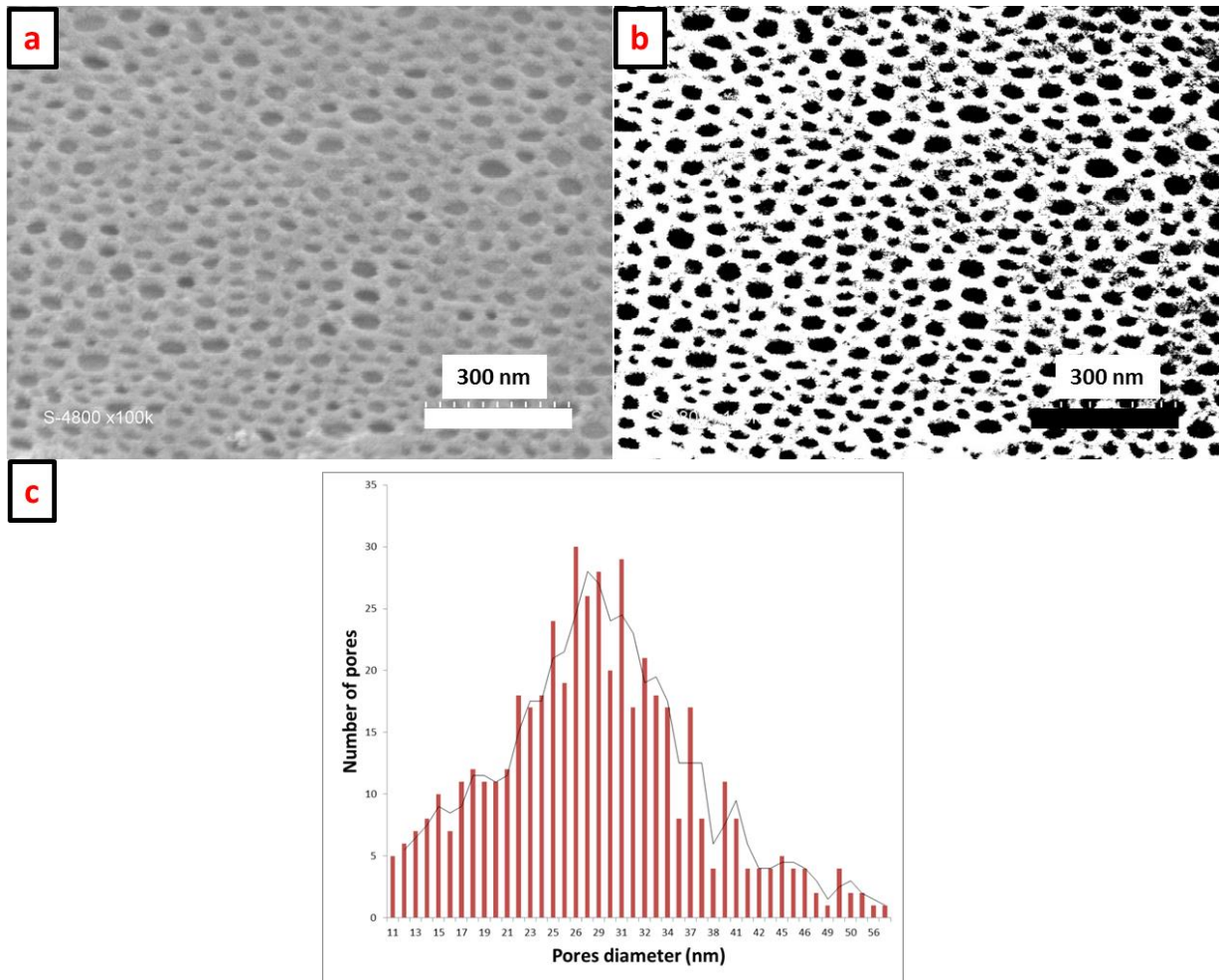


Figure S21. (a) SEM image of sample 2 after drying by spin-coating and detached from the silicon wafer by immersion in water (b) image ‘a’ binarized using Image J[®] software (c) Diagram of number of pores versus pore diameters obtained from image ‘b’ using Image J[®] software. The porosity was calculated according to $\phi = \frac{Area_{pores}}{Area_{Total\ surface}} \times 100$ giving

$$\phi = \frac{\sum_{i=1}^{89} N_{ipore} \times Area_{ipore}}{Area_{Totale}} \times 100 = 0,2869$$

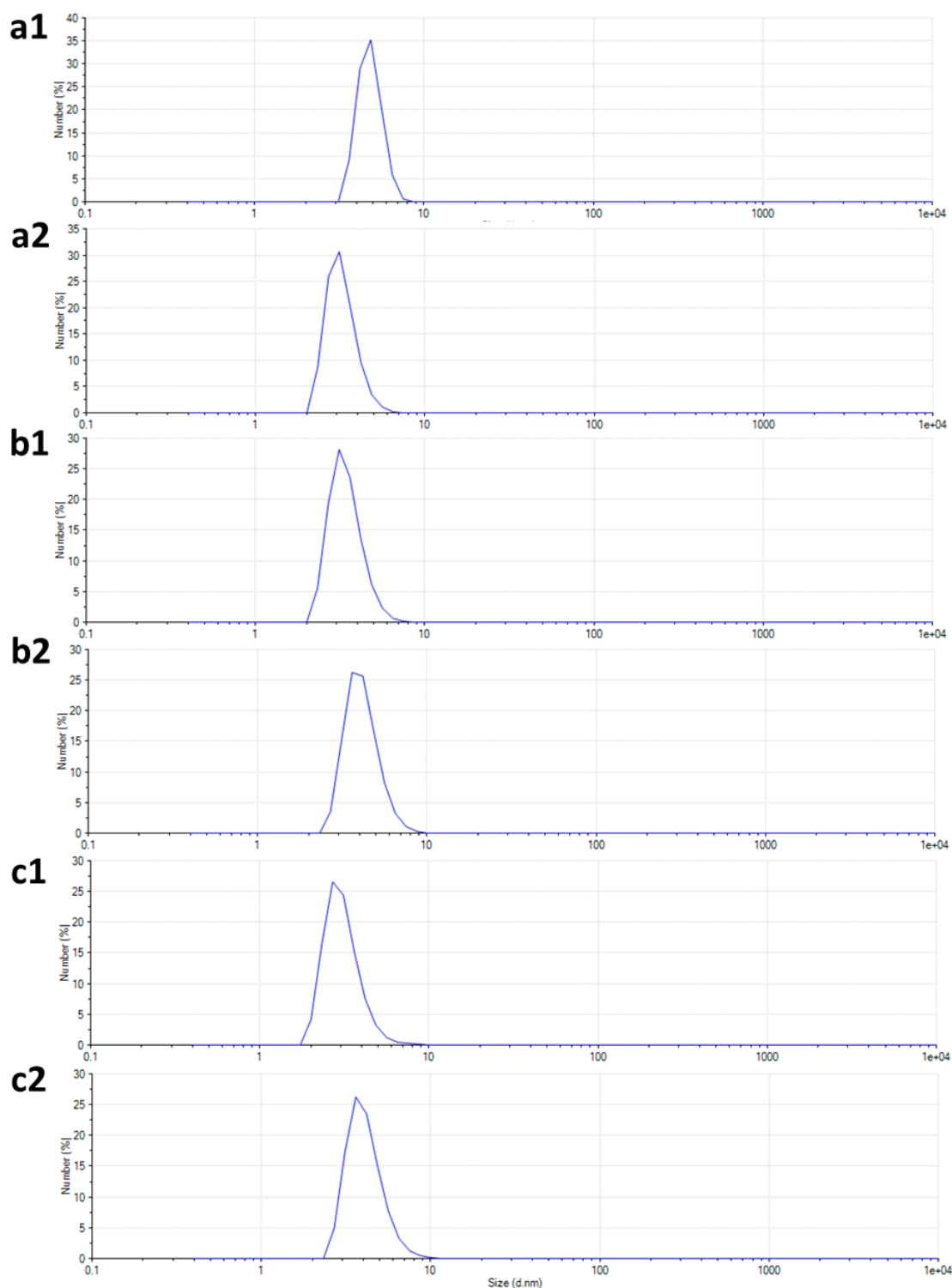


Figure S22. Dynamic Light Scattering of PS₄₈-PNaSS₂₄-PS₄₈ at different concentrations in DMF showing the absence of aggregates with only unimers detected. The letter is designing the concentration (a= 3.7 mg/ml; b= 7.8 mg/ml; c=11 mg/ml) and the number is differentiating a DLS analysis done without filtration (1) and with filtration on 0.45 μm (2).

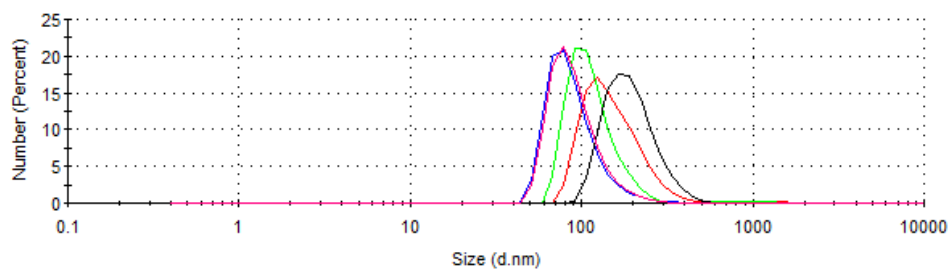


Figure S23. Dynamic Light Scattering of sample 1 at different copolymer concentrations. $C_{\text{polymer}}=5.88$ wt.%, $C_{\text{polymer}}=2.85$ wt.%, $C_{\text{polymer}}=1.47$ wt.%, $C_{\text{polymer}}=0.73$ wt.%, $C_{\text{polymer}}=0.1$ wt.%.

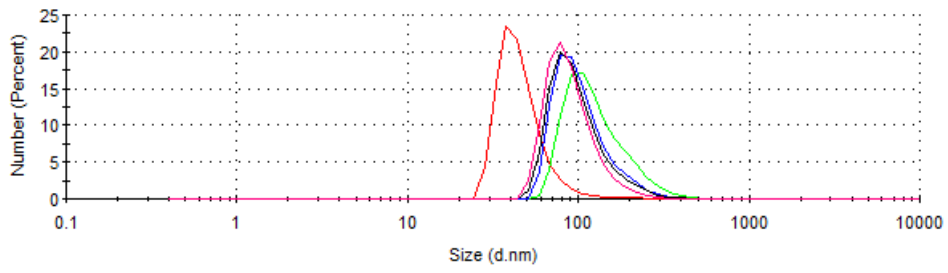


Figure S24. Dynamic Light Scattering of sample 2 at different copolymer concentrations. $C_{\text{polymer}}=5.88$ wt.%, $C_{\text{polymer}}=2.85$ wt.%, $C_{\text{polymer}}=1.47$ wt.%, $C_{\text{polymer}}=0.73$ wt.%, $C_{\text{polymer}}=0.1$ wt.%.

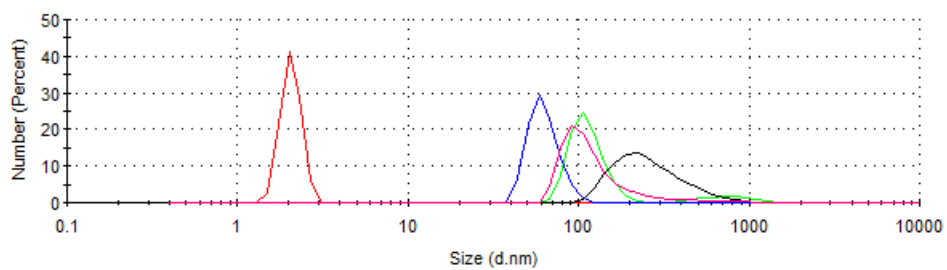


Figure S25. Dynamic Light Scattering of sample 6 at different copolymer concentrations. $C_{\text{polymer}}=5.88$ wt.%, $C_{\text{polymer}}=2.85$ wt.%, $C_{\text{polymer}}=1.47$ wt.%, $C_{\text{polymer}}=0.73$ wt.%, $C_{\text{polymer}}=0.1$ wt.%.

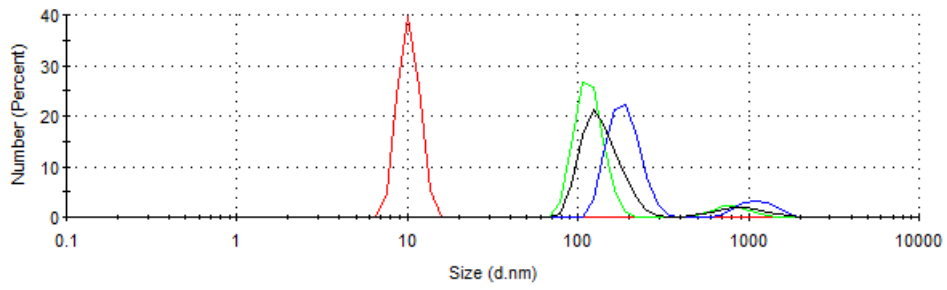


Figure S26. Dynamic Light Scattering of sample 7 at different copolymer concentrations. $C_{\text{polymer}}=5.88$ wt.%, $C_{\text{polymer}}=2.85$ wt.%, $C_{\text{polymer}}=1.47$ wt.%, $C_{\text{polymer}}=0.73$ wt.%, $C_{\text{polymer}}=0.1$ wt.%.

5. Supplementary references

1. Choi, S.-H., Lee, W. B., Lodge, T. P. & Bates, F. S. Structure of Poly(styrene-*b*-ethylene-alt-propylene) Diblock Copolymer Micelles in Binary Solvent Mixtures. *Journal of Polymer Science Part B-Polymer Physics* **54**, 22-31 (2016).
2. Kogan, V.B., Liquid-Vapor Equilibrium in the Systems Tetrahydrofuran-Water and Tetrahydrofuran-EthyleneGlycol and a Method for Dehydration of Tetrahydrofuran, *Journal of applied chemistry of the USSR* **41** 1236-1242(1968).
3. Derek, G. L., MacEwan, K., Stefan, A. & Zamari, M. Binary Mutual Diffusion Coefficients of Aqueous Cyclic Ethers at 25 °C. Tetrahydrofuran, 1,3-Dioxolane, 1,4-Dioxane, 1,3-Dioxane, Tetrahydropyran, and Trioxane, *Journal of Chemical & Engineering Data*, **45** 815-818 (2000).
4. Sun, W. *et al.* Surface-active isoporous membranes nondestructively derived from perpendicularly aligned block copolymers for size-selective separation. *Journal of Membrane Science* **466**, 229-237 (2014).